

The superprism effect in lithium niobate photonic crystals for ultra-fast, ultra-compact electro-optical switching

J. Amet^a, F.I. Baida^a, G.W. Burr^b, M.-P. Bernal^{a,*}

^a *Institut FEMTO-ST, Département d'Optique P.M. Duffieux CNRS UMR 6174, Université de Franche-Comté, 16 route de Gray, 25030 Besançon Cedex, France*

^b *IBM Almaden Research Center, 650 Harry Road, San Jose, CA 95120, USA*

Received 15 June 2007; received in revised form 1 September 2007; accepted 6 September 2007

Available online 14 September 2007

Abstract

We numerically analyze ultra-refraction and slow-light in lithium niobate photonic crystals in order to investigate and then optimize the efficiency of a tunable photonic crystal superprism. In contrast to a passive superprism 1-to-N demultiplexer, we describe a tunable bandpass filter with only three output ports. The electro-optic effect in lithium niobate is used to achieve tunability, with the filter bandwidth shifting in wavelength as the refractive index of the superprism is modified by an externally applied electric field. Such a device could be used to realize a compact and fast wavelength multiplexer/demultiplexer for telecommunications or optical interconnect applications. We calculate constant frequency dispersion contours (plane-wave expansion) to identify initial configurations that show significant ultra-refraction, and verify the expected behavior of light propagation inside the structure using 2D FDTD (finite difference time domain) simulations. We show that the voltage requirements of such an electro-optically tunable superprism could potentially be relaxed by exploiting the enhancement of the electro-optic effect recently discovered by our group [M. Roussey, M.-P. Bernal, N. Courjal, D. Van Labeke, F.I. Baida, Electro-optic effect exaltation on lithium niobate photonic crystals due to slow photons. *Appl. Phys. Lett.* 89 (24) (2006) 241110], which we believe to be due to the presence of slow-light in the nanostructure. We present a methodology that readily identifies superprism design points showing both strong ultra-refraction as well as low group velocity. However, we find that this improved voltage efficiency comes at the cost of reduced operating bandwidth and increased insertion losses due to proximity to the band-edge.

© 2007 Elsevier B.V. All rights reserved.

PACS : 42.70.Qs; 42.82. –m; 78.20.Jq

Keywords: Photonic crystals; Electro-optic effect; Superprism effect; Lithium niobate

1. Introduction

Photonic crystals are periodic dielectric structures of strong index contrast that make it possible to manipulate and control light in devices as small as a few

wavelengths in size. Having become a widely studied subject in the photonics community, many phenomena such as perfect mirrors, photonic crystal waveguides, and nano-cavities [2–4] have been discovered and subsequently explored.

One intriguing property found in photonic crystals is an unusual frequency dependence of the direction of light propagation inside the photonic crystal [5]. This behavior was first reported in three-dimensional (3D) photonic crystals fabricated in SiO₂/Si and was

* Corresponding author. Tel.: +33 3 81 66 64 10; fax: +33 3 81 66 64 23.

E-mail address: maria-pilar.bernal@univ-fcomte.fr (M.P. Bernal).

called the “superprism” phenomenon [6]. These peculiar dispersion properties have motivated a number of new micro-optical components such as superlenses [7,8], negative refraction devices [7,9], and wavelength multiplexing/demultiplexing devices [10,11]. Such devices, the latter in particular, are of great interest for optical processing and communications due to the possibility of separating the wavelengths of an optical signal with a compact device using ultra-refraction. While most of the first devices proposed were passive, requiring the incident angle or wavelength to be varied externally, more recent works have introduced active superprism devices. Here, the input angle and wavelength can stay fixed, yet the propagation angle within the device varies rapidly with small changes in the refractive index of some portion of the photonic crystal structure. Theoretical design studies for tunable superprism devices have been published based on both electro-optical [12,13] as well as liquid-crystal [14] or nonlinear [15] materials.

In this work, we numerically investigate the superprism effect for an index-tunable photonic crystal located within a conventional lithium niobate planar or stripe waveguide. First of all, we introduce the concept of a tunable bandpass filter utilizing the superprism effect. Then we briefly describe the electro-optic effect in lithium niobate, and the possibility for enhancement in the presence of slow light. Constant frequency dispersion contours for a design point offering strong ultra-refraction are discussed, and the operation of the tunable bandpass filter is investigated using 2D finite difference time domain (FDTD) numerical simulations. In order to further investigate and then exploit the enhancement of the electro-optic effect by slow-light within the photonic crystal nanostructure, we present a methodology that readily identifies superprism design points showing both strong ultra-refraction as well as low group velocity. We find that this improved voltage efficiency comes at the cost of reduced operating bandwidth and increased insertion losses due to proximity to the band-edge. We conclude that the experimental characterization of both the wavelength and index sensitivities of such a photonic crystal superprism will be needed to provide improved understanding of the electro-optic enhancement in nanostructured lithium niobate. With such knowledge, the tradeoff between voltage efficiency and bandwidth can be quantified, leading to ultra-fast, ultra-compact tunable bandpass filters in lithium niobate using the superprism effect.

2. Active superprism devices as tunable wavelength filters

Conventionally, the application most frequently discussed with the superprism effect is a 1-to-N demultiplexer [16,10,11], as shown schematically in Fig. 1(a). Here, different wavelength-multiplexed signals are split into a static distribution of distinct output ports. When used in reverse, such a device becomes a multiplexer. Theoretically, a photonic crystal superprism should allow such a device to be quite compact because of ultra-refraction (the angle at which light is refracted changes rapidly with wavelength). However, as numerous authors have shown, inherent tradeoffs between the size and spatial-frequency content of beams within a superprism device tend to impose a limit on the number of possible output channels [16,10,11,17,18]. Various alternative designs have been introduced [17,18] which can increase the number of output ports by combining negative refraction inside the photonic crystal together with normal diffraction outside the device. However, these approaches tend to increase the overall device footprint.

In contrast, we propose a tunable photonic crystal superprism device with only a small number of output ports, to be used as a tunable wavelength filter. For instance, the three-port voltage-controlled device shown in Fig. 1(b) acts as a tunable bandpass filter. A two-port device could serve as a tunable high-pass filter. When the operating voltage is zero, the filter selects out one narrow wavelength band into the center output port, deflecting lower wavelengths into the upper port and higher wavelengths into the lower port. But as the operating voltage is changed, the particular wavelength band dropped into the center port can be tuned up or down. When operated in reverse, such a device would implement a tunable wavelength combiner. The functionality of the passive demultiplexer shown in Fig. 1(a), as well as many other interesting routing scenarios, could be implemented simply by cascading a small number of such active superprism wavelength filters.

Passive and active superprism devices share many features and requirements. Large angle deflection with small changes in wavelength are still necessary, and both devices would need to offer low insertion losses and minimal crosstalk between ports in order to be truly interesting. Fortunately, as we show below, configurations that would make good passive superprism devices (large angle swing with wavelength change) also make good active devices (large angle swing with change in refractive index). However, since the number of desired

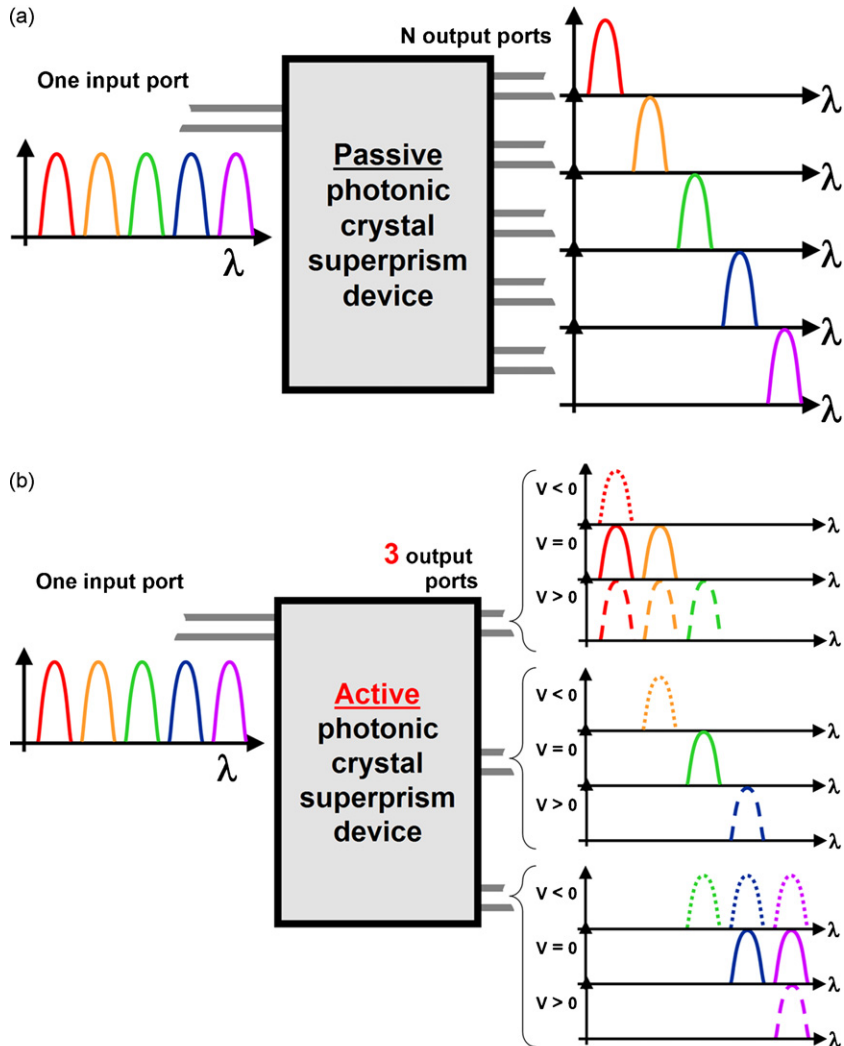


Fig. 1. A prototypical application for a passive superprism device is a 1-to-N multiplexer/demultiplexer (a), in which ultra-refraction allows different wavelengths to be statically routed to output ports within a compact footprint [16,10,11]. In contrast, we propose here a tunable bandpass-filter (b), utilizing the superprism effect to steer input signals to one of three output ports. The wavelength dropped into the center port changes as the operating voltage tunes the index of refraction of the photonic crystal device.

output paths is much smaller, the tradeoff imposed by beam diffraction is much less crucial to the success of the device. Instead, a critical aspect becomes the practicality of imposing sufficiently large changes in index of refraction, either through changes in voltage or some other suitable control variable.

3. Electro-optic effect in lithium niobate and its enhancement by nanostructure

The combination of excellent electro-optical, acousto-optical, nonlinear optical and piezoelectric properties together with chemical and mechanical

stability makes lithium niobate an ideal material for integrated optoelectronics. In particular, lithium niobate is widely used to fabricate high speed modulators, waveguide devices, dispersion compensators, waveform converters and parametric amplifiers [19]. Furthermore, nano-structuring of this material, while not trivial, is possible by focused ion beam etching [20]. Recently, a square-lattice lithium niobate photonic crystal was fabricated and experimentally demonstrated as an electro-optically tunable filter [21].

The electro-optic effect is the change in the refractive index of a material induced by an applied external

electric field, quantified as

$$\Delta\left(\frac{1}{n^2}\right)_{ij} = \sum r_{ijk} E_k, \quad (1)$$

$$r_{ijk} = \begin{pmatrix} 0 & -r_{22} & r_{13} \\ 0 & r_{22} & r_{13} \\ 0 & 0 & r_{33} \\ 0 & r_{51} & 0 \\ r_{51} & 0 & 0 \\ -r_{22} & 0 & 0 \end{pmatrix}$$

where n is the material refractive index, E_k the electric field components, and r_{ijk} represents the electro-optic tensor of the material [22]. The electro-optic device in lithium niobate is inherently extremely fast, with commercial modulators of 40 GHz now widely available [23].

For lithium niobate, in order to maximize the modification of the refractive index, we use the strongest electro-optical coefficient: r_{33} (~ 32.2 pm/V at $0.633 \mu\text{m}$) [23]. This can be practically achieved by applying an electric field along the z -axis (crystal symmetry axis) of a uniaxial lithium niobate crystal. When this particular applied field modifies the extraordinary refractive index of the material, Eq. (1) can be simplified to:

$$\Delta n_e = -\frac{1}{2} n_e^3 r_{33} E_3, \quad (2)$$

which is widely known as the Pockel's equation [23]. In the case of lithium niobate, a variation of the refractive index of only $\Delta n = 0.01$ would require a fairly large applied field of $66 \text{ V}/\mu\text{m}$.

However, we have recently observed experimentally that this high voltage requirement is somehow greatly reduced in lithium niobate photonic crystals. We recently fabricated and characterized an electro-optical modulator based on a square lattice of air holes within a lithium niobate annealed proton exchange (APE) waveguide [1]. An electro-optic effect 300 times larger than for bulk lithium niobate was observed [1]. We believe that this effect is due to the much lower group velocity of the light propagating inside the nanostructured lithium niobate structure. We have been able to theoretically predict nearly the same enhancement factor that we observe experimentally [24]. To do so, we introduced the local field factor f , previously used to describe enhanced nonlinear optical coefficients in photonic crystals [25,26], into the Pockel's equation. As described in Ref. [24], this modified Pockel's equation

would take the form

$$\Delta n_e = -\frac{1}{2} n_e^3 r_{33} E_3 f^3. \quad (3)$$

The local field factor f then quantifies the enhancement to the normal electro-optic effect due to increased interaction between the slow light and the electro-optical material.

While this treatment has the satisfying aspect of matching the experimental observations, it is likely that significant further investigations will be necessary before the exact nature of the observed enhancement is fully understood. For instance, although the motivation for the exponent of f in Eq. (3) is the presence of three electric fields, one of those fields is the applied dc field. Thus, the main support behind the exponent of f becomes the match to experiment. In any case, at this point the only facts of which we can be quite sure are that such an enhanced electro-optic effect is possible, and that we can increase the degree of enhancement by working in a slow-light regime. As such, we can use the local field factor f as a metric to find a design point which should lead to a strong enhancement.

The local field factor f can be computed theoretically in several ways. The preferred method is to spatially integrate the enhanced electric field within the structure as computed by FDTD, since this takes into account the finite dimensions of the actual device [24–26]. However, an estimated local field factor f_{PWE} can be obtained by simply comparing the group velocity within the photonic crystal (as computed by the plane-wave expansion (PWE)) to the bulk group velocity, as

$$f_{\text{PWE}} = \sqrt{\frac{v_g^{\text{BULK}}}{v_g^{\text{PC}}}}, \quad (4)$$

where v_g^{BULK} is the group velocity in the bulk lithium niobate (e.g., c/n_e) and v_g^{PC} is the group velocity within the nanostructured lithium niobate photonic crystal [24–26]. Because, the PWE assumes an infinitely large structure, this number will tend to differ from the actual field factor. For instance, right at the band-edge f_{PWE} will grow without bound as the group velocity goes to zero. However, we have found previously [24] that in general the value of f_{PWE} tends to be smaller than the value of f obtained by field integration [27]. In any case, we can expect that the trend in f_{PWE} will closely follow the trend in the real field factor f .

The study of simple dispersion diagrams for our intended photonic crystal superprism should allow us to identify a configuration offering slow-light propagation. Where v_g^{PC} , manifesting as the slope of the bands in the

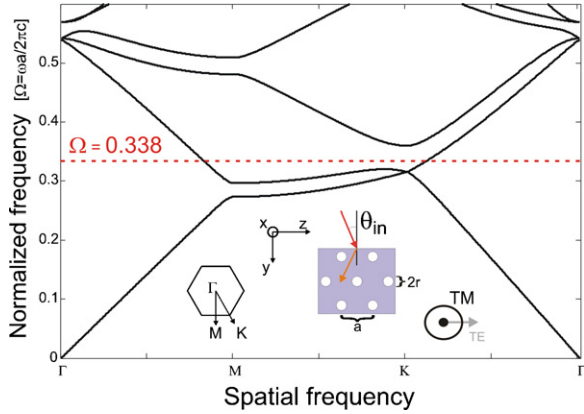


Fig. 2. Band diagram for an infinite photonic crystal in a triangular lattice ($a = 525$ nm, $r = 105$ nm) of air holes ($n = 1$) for a lithium niobate substrate ($n_e = 2.143$) and TM polarization (electric field parallel to the cylindrical axis of the holes). The red line represents the normalized frequency of $\Omega = 0.338$ (equivalent to $\lambda = 1.55$ μm when $a = 524$ nm) corresponding to Fig. 3. Also shown is a schematic view of the triangular lattice photonic crystal in both real and frequency space.

dispersion diagram, tends to zero, then f_{PWE} will become very large and we can expect the real value of f to be substantial as well. In such a case, based on our previous experimental observations [1,24], we should be able to greatly improve the efficiency with which the electro-optic effect modifies the refractive index through external field, enabling the realization of ultra-compact electro-optic superprism devices.

4. Electro-optically tunable superprism

Our overall goal is to find a set of parameters for an electro-optic photonic crystal superprism device that is efficiently tunable, yet which will also be feasible to fabricate. Two different configurations are compared: the first, based on the standard Pockel’s equation (Eq. (2)), has been selected for good ultra-refraction behavior but with no consideration of group velocity. Thus, as will be shown, this first configuration requires a high external voltage for significant angle swings. The second configuration has been found with the additional requirement of a high local field factor f_{PWE} (low group velocity), so that the external voltage needed for the same beam steering can be significantly reduced. In this work, we only take into account TM polarization (the electric field vector parallel to the cylindrical axis of the holes). This corresponds to a photonic crystal fabricated on a X-cut crystal of lithium niobate in which a planar or stripe waveguide has been created by in-diffusion of titanium [28].

We choose to work with a triangular lattice of air holes in order to achieve strong ultra-refraction, a reasonable hole-size amenable to a realistic fabrication process, and a structure with a low air-fraction in order to maximize the effect of changes in substrate index. The dispersion diagram of this 2D photonic crystal obtained with the PWE method [29,30] is shown in Fig. 2 for $r/a = 0.2$, where a is the lattice periodicity

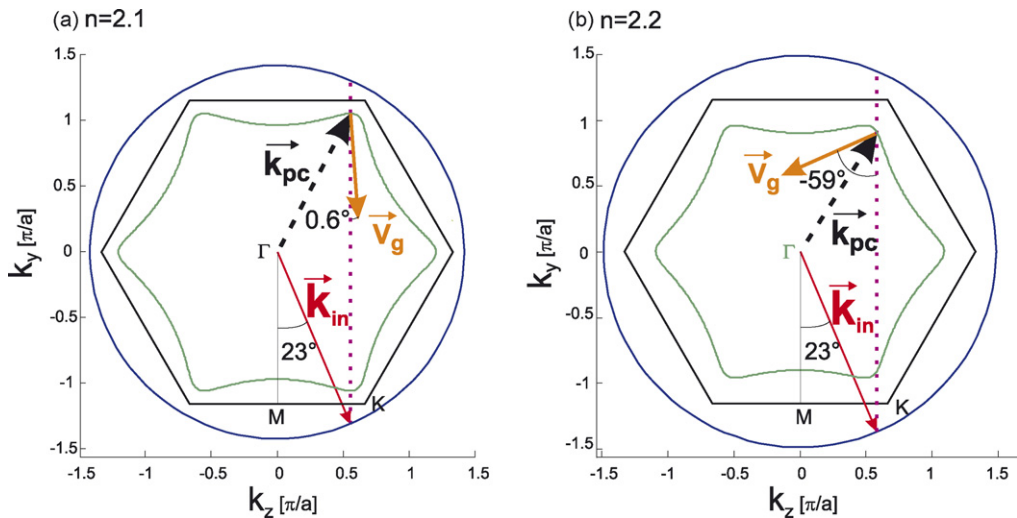


Fig. 3. Constant frequency dispersion surfaces for a triangular lattice of circular air holes in lithium niobate substrate ($a = 525$ nm, $r = 105$ nm). The incident angle is fixed at 23° from the ΓM direction and the incident wavelength is $\lambda = 1.55$ μm ($\Omega = 0.338$ for $a = 524$ nm). In (a), when the external applied electrical field is sufficient to reduce the refractive index of the lithium niobate to $n = 2.1$, the power flow inside the photonic crystal is at an angle of 0.6° from the ΓM direction. In contrast, when the sign of the external electrical field is inverted to increase the refractive index from its zero-voltage value of 2.143 up to $n = 2.2$ (b), the group velocity is at an angle of -59° .

and r is the hole radius. Note that the cardinal directions have been chosen here to correspond correctly to the required crystal axes of the lithium niobate substrate. At the normalized frequency $\Omega = \omega a/2\pi c = a/\lambda = 0.338$ marked by the red dashed line, the propagating Bloch mode is located in the second lower band.

The constant frequency dispersion contours at this normalized frequency (Fig. 3(a)) exhibit a hexagonal shape that clearly present some interesting regions [31]. In particular, near the K point(s) of the Brillouin zone the dispersion contour bends sharply with spatial frequency. To couple into this spatial frequency inside the photonic crystal, we can illuminate the ΓK interface of the photonic crystal at an incident angle of 23° from the ΓM direction. Conservation of the k_z component determines the wavevector \mathbf{k}_{PC} in the photonic crystal, while the direction of the group velocity vector, \mathbf{v}_g , is perpendicular to the tangent of the dispersion surface [31]. The magnitude of the group velocity can be obtained by using frequency contours at nearby normalized frequencies to compute the gradient $\nabla_k \omega$ at this operating point (k_x, k_y, Ω) . Although the use of the PWE method and vectors lying on dispersion contours implies an infinitely wide input beam, this assumption is a reasonable first approximation given that the stripe lithium niobate waveguides we typically use are $\sim 7 \mu\text{m}$ in width (approximately $10\times$ larger than λ/n_e).

The operation of previous superprism devices depended on the fact that the dispersion contours of constant frequency (in both the bulk and the photonic crystal) change when either the refractive index or the wavelength vary. But the tunable bandpass filter described in Fig. 1 requires *both* of these effects. At a constant wavelength, we want to be able to steer light to a particular output port depending on the particular index of refraction, as imposed by the control voltage. However, for a given applied voltage, we also want different wavelengths to steer to different ports. Here we use constant frequency contours to check that both of these effects are present with sufficiently large angle changes.

Fig. 3 shows two constant frequency dispersion curves for a constant input wavelength (normalized frequency $\Omega = 0.338$, corresponding to $\lambda = 1.55 \mu\text{m}$ if $a = 525 \text{ nm}$). Using an incident angle of 23° , upon a decrease in refractive index to $n = 2.1$ due to the application of a large external electric field (Fig. 3(a)), the group velocity vector associated with power flow inside the photonic crystal is at an angle of 0.6° (from the ΓM direction). However, if the refractive index increases to $n = 2.2$, then the angle of the group

velocity vector is -59° (Fig. 3(b)). Fig. 4 shows the continuous change in group velocity direction as the index is varied from $n = 2.1$ to 2.2 . According to Eq. (2), this index variation would require an applied electric field of $660 \text{ V}/\mu\text{m}$, as shown on the upper horizontal axis of Fig. 4. Thus, if no special precautions are taken in choosing the design point, the angular sensitivity is $\sim 13^\circ$ for a refractive index variation of 1%. This corresponds to $\sim 13^\circ$ for a change in applied electric field of $+140 \text{ V}/\mu\text{m}$. This calculated index sensitivity is approximately the same as that predicted for PLZT devices [12,13].

Just as a passive superprism device is used as a wavelength demultiplexer, the active superprism device described in Fig. 1(b) also needs to be able to steer beams solely on the basis of wavelength (at constant index of refraction). In Fig. 5, constant frequency contours are shown for two different normalized frequencies ($\Omega = 0.350$ and 0.328), corresponding to 1.5 and $1.6 \mu\text{m}$ for an appropriate choice of a (525 nm). With light incident at 23° , the direction of the light inside the photonic crystal is equal to -70° for $\lambda = 1.5 \mu\text{m}$, and to 10° for $\lambda = 1.6 \mu\text{m}$ (angles measured from the ΓM direction). The sensitivity of our device can be estimated to be $\sim 0.8^\circ/\text{nm}$, roughly the same order of magnitude as found in earlier work on passive superprisms [32–34].

It would seem that the continuous angle deflection shown in Fig. 4 would be incompatible with abrupt

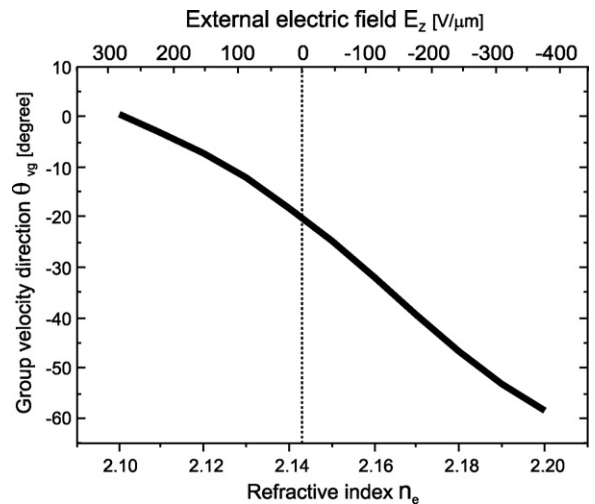


Fig. 4. Angle of the group velocity vector within a lithium niobate triangular lattice photonic crystal as a function of both refractive index n_e and external electric field E_z , for the configuration described in Fig. 3. The scaling from index change to electric field is performed with the conventional Pockel's equation, Eq. (2). An angle change of 60° occurs for a 4.67% change in index of refraction, requiring a change in external field of $660 \text{ V}/\mu\text{m}$.

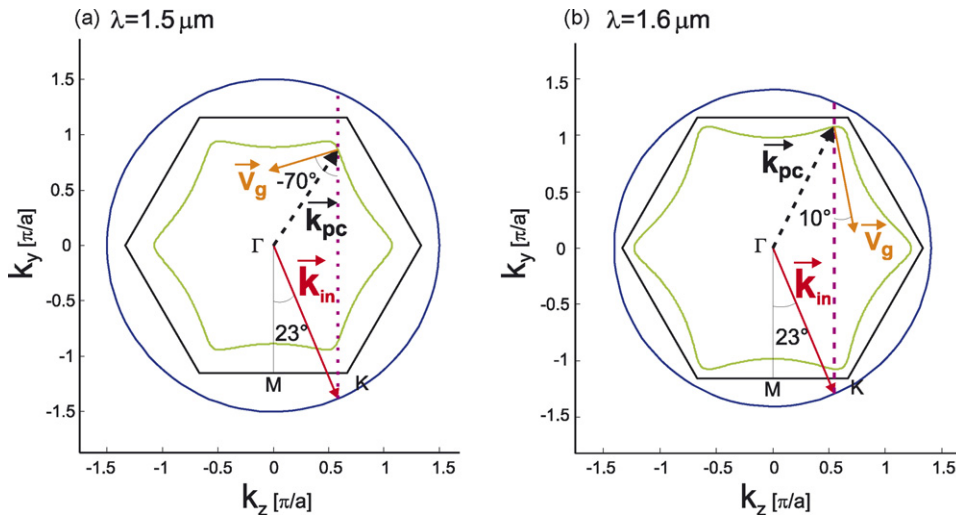


Fig. 5. Constant frequency dispersion surfaces for a triangular lattice of circular air holes in lithium niobate substrate with no applied voltage ($a = 525 \text{ nm}$, $r = 105 \text{ nm}$, $n = 2.143$). When the incident angle is fixed at 23° from the ΓM direction, an incident wavelength of $\lambda = 1.5 \text{ }\mu\text{m}$ (a), $\Omega = 0.350$ for $a = 525 \text{ nm}$) couples into a wavefront inside the photonic crystal with power flow at an angle of -70° from the ΓM direction. In contrast, an incident wavelength of $\lambda = 1.6 \text{ }\mu\text{m}$ (b), $\Omega = 0.328$) corresponds to a group velocity at an angle of 10° .

switching of light from one output port into another. However, we show with 2D finite difference time domain (FDTD) simulations that we can in fact implement the tunable bandpass filter described by Fig. 1(b) with the same design point represented by Figs. 3–5.

We perform FDTD simulations with a Gaussian beam of $7\text{-}\mu\text{m}$ width incident on 25×20 air holes arranged in a triangular lattice photonic crystal ($r/a = 0.2$, $a = 524 \text{ nm}$). The ΓK interface is tilted

by 23° with respect to the input beam. The $7\text{-}\mu\text{m}$ beam width corresponds to the output mode of a stripe waveguide fabricated by titanium diffusion into the top surface of a lithium niobate substrate. Although these are 2D simulations, in a real device light would be confined vertically to a depth of $2\text{--}3 \text{ }\mu\text{m}$ below the substrate surface by the gradient index profile introduced by titanium in-diffusion. Thus, as long as the holes are deep enough to interact with this mode, these 2D simulations should still be quite descriptive of the

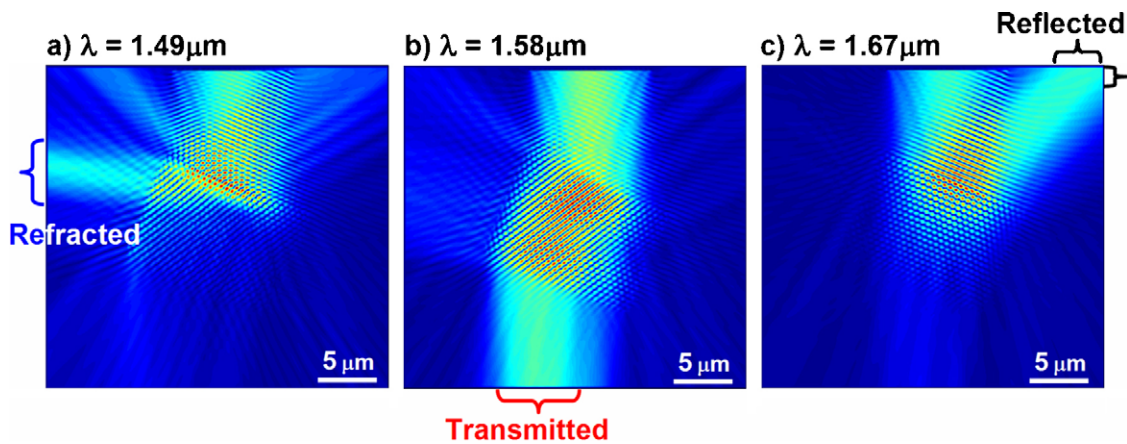


Fig. 6. Out-of-plane electric field amplitude as calculated by 2D FDTD for a triangular lattice of 25×20 circular air holes in a lithium niobate substrate. The structure is rotated so that light with an initial spatial Gaussian profile of $7 \text{ }\mu\text{m}$ width is incident at an angle of 23° from the ΓM direction. As in Fig. 3, $a = 525 \text{ nm}$, $r = 105 \text{ nm}$, and the index of the lithium niobate substrate is $n = 2.143$. Part (a) corresponds to an incident wavelength of $\lambda = 1.49 \text{ }\mu\text{m}$, for which most of the power is refracted by a large (negative) angle. Part (b) corresponds to $\lambda = 1.58 \text{ }\mu\text{m}$ where most of the light is transmitted through the crystal with only a small refraction angle. In Part (c), the incident wavelength of $\lambda = 1.67 \text{ }\mu\text{m}$ falls into the stop-band, so that most of the light reflects from the photonic crystal.

performance of a real device. At the boundaries of the simulation, perfectly matched layers (PML) are used to avoid parasitic reflections of outgoing radiation [35].

Fig. 6 shows the amplitude of the out-of-plane electric field for three different wavelengths (1.49, 1.58, and 1.67 μm) at the index of refraction corresponding to zero applied voltage ($n = 2.143$). At the lower wavelength (Fig. 6(a)), corresponding closely to the configuration shown in Fig. 5(a), the incoming beam undergoes negative refraction by a large angle, exiting the left face of the photonic crystal. At an intermediate wavelength (Fig. 6(b)), corresponding roughly to Fig. 5(b), the incoming beam is refracted by a very small angle, passes through the photonic crystal and exits the lower face to continue as a transmitted beam. Finally at a large enough wavelength (Fig. 6(c)), the band-edge is reached and the signal is reflected from the outer boundary of the photonic crystal. Thus, the third output port of our tunable bandpass filter is due to the band-edge of the photonic crystal, and the superprism effect is used to separate the first two output ports (“refracted” and “transmitted”).

It turns out that the total internal reflection along the left edge of the photonic crystal helps to make the transition between these two output ports much sharper than might be suggested by the continuous angle deflection shown in Fig. 4. In order to quantify this, we use the three different output ports marked on Fig. 6 in order to measure the response of our tunable bandpass filter. A number of 2D FDTD simulations were run to cover a range of wavelengths at three different indices of refraction. Distinct CW simulations were used rather than one pulsed simulation in order to provide field distributions and to gauge the effect of changing the size and position of the output ports. The power passing through the three marked regions was tabulated for each output port and is shown in Fig. 7, normalized to the maximum transmitted power. At any given index of refraction, a narrow band of wavelengths passes through the center “transmit” port. As the index of refraction of the lithium niobate changes from $n = 2.1$ to 2.2, the wavelength of peak transmission in this port shifts by nearly 80 nm. The overall operating span of the device is nearly 300 nm.

These FDTD simulations not only verify that the design point identified by PWE is correct, but also show that even in the presence of the finite-width beams of experimental interest to us, the desired ultra-refraction effect still works well. But, while the resemblance of Fig. 7 to the desired characteristics described in Fig. 1(b) is quite satisfying, there are still some aspects in which further improvement is needed. Although the

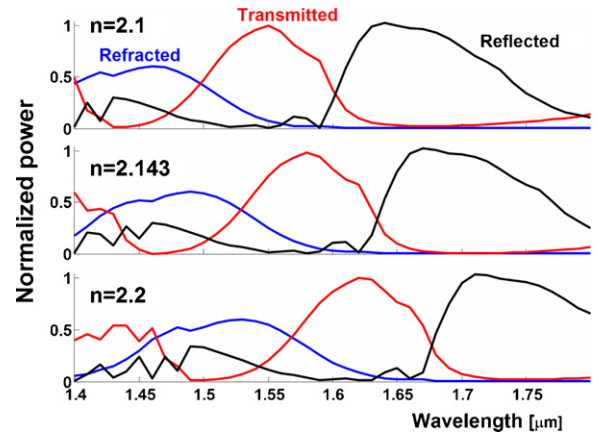


Fig. 7. The operation of a lithium niobate active superprism as a tunable bandpass filter is illustrated by the normalized power received in three different output ports, for 2D FDTD simulations at three different indices of refraction. At a constant index of refraction (corresponding to a particular operating voltage), the device splits different wavelengths into one of three output ports. As the index of refraction is increased, the position of this band increases in wavelength. The location and approximate size of the three output ports are illustrated in context on Fig. 6. Each output port is roughly the same size (7–9 μm wide) as the assumed width of the input port. Output power is normalized to the maximum received in the transmitted port.

crosstalk in the reflected port is fairly low, the transitions between channels are not as sharp as would be needed for a practical device. For the transition between refracted and transmitted channel, this might be simply a matter of adding more rows in order to sharpen the cutoff at the band-edge. However, sharpening the transition from transmitted to refracted will involve understanding the exact role of the apparent total internal reflection at the left edge of the photonic crystal. In addition, there is a significant amount of crosstalk into the reflected channel at wavelengths that ought to be deflected into the refracted port. This crosstalk, as well as other stray back-reflected light not entering one of the three output ports, is clearly visible in Fig. 6(a). Here, modification of the input interface [36,17] may be possible in order to reduce the loss and crosstalk in this wavelength regime.

We note that the size of the output ports used here are almost exactly the same size as the width of the input waveguide (7–9 μm in width). This clearly shows the minor role played by beam diffraction in an active superprism device, because of the small number of output ports. In fact, it would seem that the design point chosen here is already a reasonably good tunable bandpass filter, with various design changes possible for sharpening up the channel transitions, reducing crosstalk and decreasing overall insertion loss. However, the total change in refractive index is identical to that shown

in Fig. 4. Thus, the standard Pockel’s equation would predict that in order to implement the device shown in Fig. 7, we would need to apply electric fields as large as $\pm 330 \text{ V}/\mu\text{m}$ across the device. In the remainder of the paper, we try to find design points that might help reduce this voltage swing by combining strong ultra-refraction together with slow-light enhancement of the electro-optic effect.

5. Electro-optically tunable superprism enhanced by slow-light

Our objective now is to try to reduce operating voltages by moving our tunable superprism design into a regime where the electro-optic effect will be enhanced by slow light propagation. So, we need to find a suitable configuration in which both slow light and a strong ultra-refraction effect are both present. This would allow us to design a tunable superprism device that would be both sub-millimeter in size and low-voltage.

To aid in our search for a suitable design point, we perform multiple PWE computations across a range of r/a , n , θ_{in} , and normalized frequency Ω , for both ΓK

and ΓM lattice termination. For each of these many design configurations, we compute both θ_{v_g} and f_{PWE} . We are looking for design points where a small change in index changes θ_{v_g} by a large amount and the group velocity is low (as quantified by a large f_{PWE}). We can compactly examine this set of results in the form of two-dimensional design maps. Shown in Fig. 8 are the calculated group velocity direction θ_{v_g} (Fig. 8(a)) and local field factor f_{PWE} (Fig. 8(b)), parameterized in color as a function of the normalized frequency Ω and incident angle θ_{in} , for one particular hole radius ($r/a = 0.2$), index of refraction ($n = 2.143$), and lattice orientation (lattice terminated along ΓK). Just by themselves, these maps are quite informative, since rapid color changes on the first (Fig. 8(a)) identify regions where the dispersion curves change curvature rapidly (thus leading to strong ultra-refraction), while the other (Fig. 8(b)) identifies band-edges where group velocity falls abruptly (thus leading to large f_{PWE}).

The smallest value of f_{PWE} , corresponding to the upper bound on group velocity within the photonic crystal, might be expected to be slightly lower than the index of refraction of bulk lithium niobate because a small fraction (14.5%) of the device is air. From a weighted sum of these two indices, we obtain a lower bound on f_{PWE} of 0.96. In practice, the lowest value of f_{PWE} we calculate is approximately 0.99. The field factor values f_{PWE} then increase to larger values near the band-edges of the photonic crystal due to the presence of slow-light. However, there are some parameter combinations where no relevant superprism solution is possible (marked on both Fig. 8(a) and (b) in gray), as well as

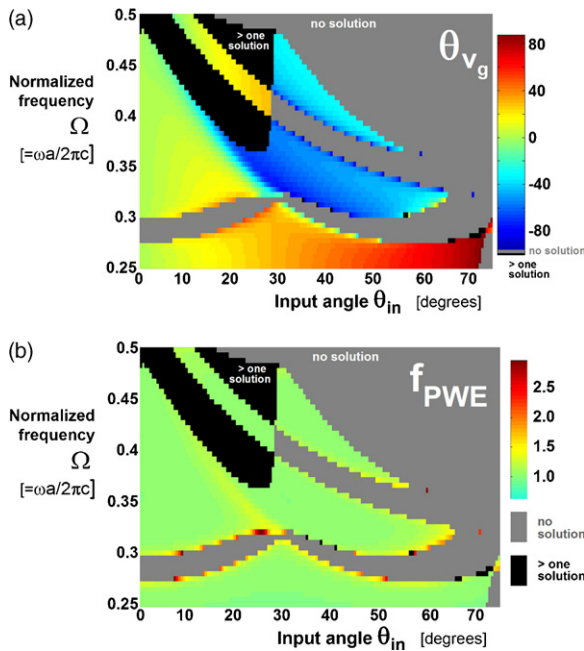


Fig. 8. Group velocity direction θ_{v_g} (a) and local field factor f_{PWE} (b), as calculated by the PWE algorithm and parameterized in color as a function of the normalized frequency Ω and incident angle θ_{in} , for a particular hole radius ($r/a = 0.2$), index of refraction ($n = 2.143$), and lattice orientation (lattice terminated along ΓK). Design configurations offering no photonic crystal mode to couple into, or more than one photonic crystal mode to couple into, are shown in gray and black, respectively.

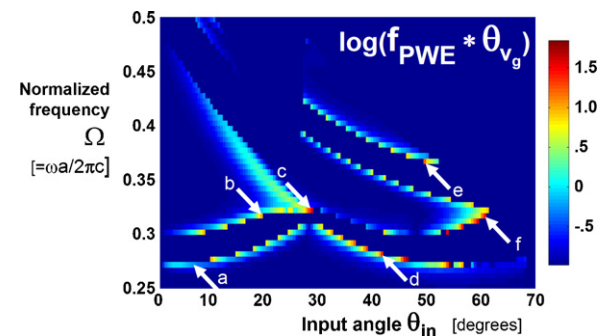


Fig. 9. Design metric for slow-light ultra-refraction with $r/a = 0.2$ and ΓK lattice termination, defined as $\log((1/2)(f_{\text{PWE}}^{n_1} + f_{\text{PWE}}^{n_2})|\theta_{v_g}^{n_2} - \theta_{v_g}^{n_1}|)$, created by combining the pair of design maps shown in Fig. 8 for $n_1 = 2.143$ together with a similar pair (not shown) corresponding to $n_2 = 2.160$. The logarithm is used only to help the linear colormap show both excellent (red) and moderately good (yellow) design solutions. Six interesting design configurations are identified with white arrows, with corresponding constant frequency dispersion surfaces shown in Fig. 10(a–f).

regions where more than one relevant superprism solution is possible. Since these design points would lead to refraction of multiple beams within the photonic crystal, we remove these from consideration as well (regions colored black on both Fig. 8(a) and (b)).

By taking both the pair of design maps shown in Fig. 8 for index of refraction n_1 , together with the pair corresponding to a different index of refraction n_2 , we can compute an overall slow-light superprism design metric, defined as

$$\log \left(\frac{f_{\text{PWE}}^{m_1} + f_{\text{PWE}}^{m_2}}{2} |\theta_{v_g}^{n_2} - \theta_{v_g}^{m_1}| \right). \quad (5)$$

This design metric is shown parameterized in color in Fig. 9, for $n_1 = 2.143$ and 2.160 . This equation simply quantifies the idea that we are looking for design configurations where the group velocity stays low (high f_{PWE}) and the angle-change induced by refractive index change is also large. The logarithm is used only to help the linear colormap show both excellent (red) and moderately good (green and yellow) design solutions. Note that for the gray and black regions corresponding to zero and more than one superprism solutions, respectively, we have simply set the design metric to a very low number (dark blue) so as to avoid such design configurations.

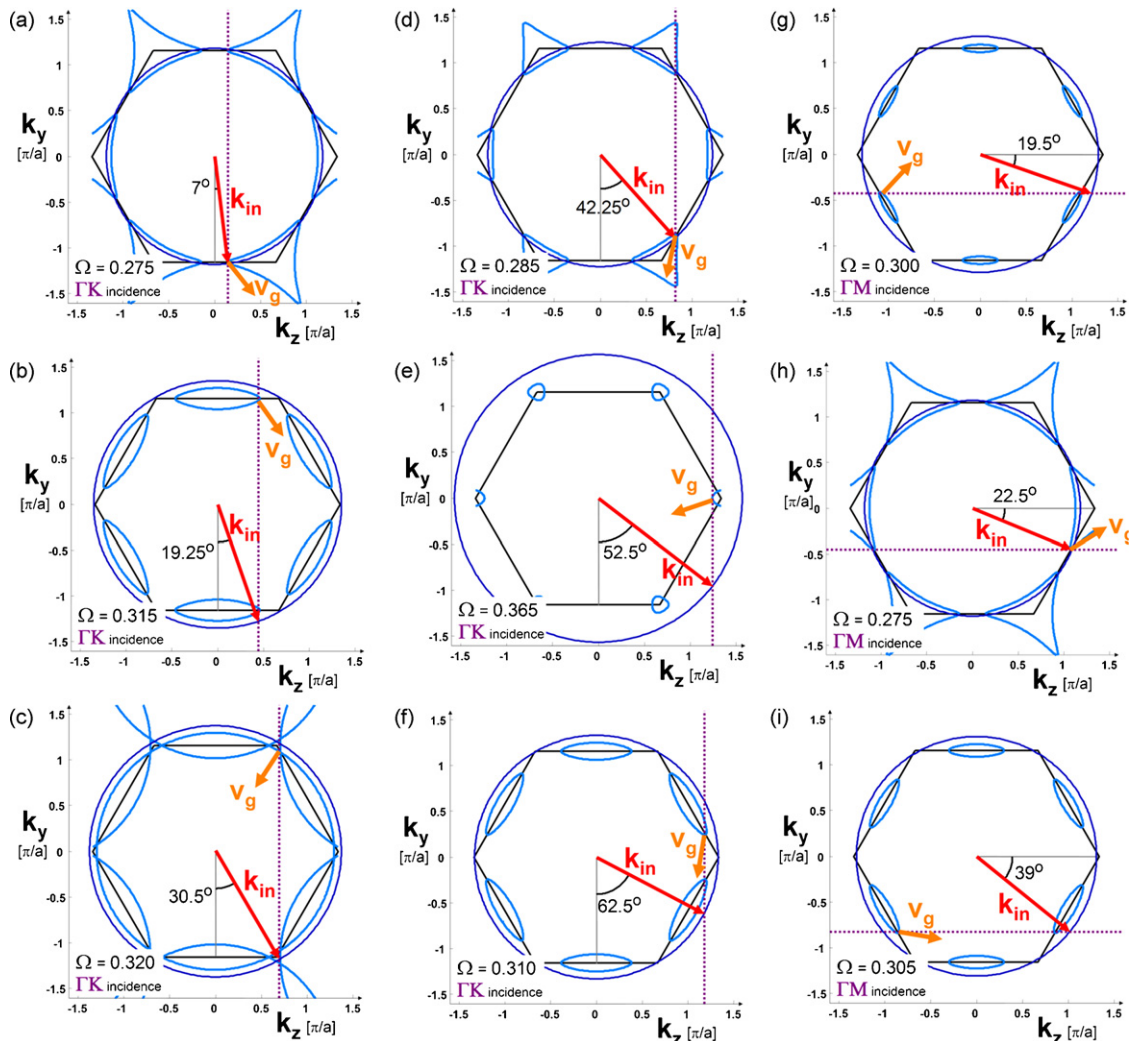


Fig. 10. Constant frequency dispersion surfaces for a triangular lattice of circular air holes in lithium niobate substrate, corresponding to (a–f) the six interesting design configurations identified in Fig. 9; as well as to (g–i) three additional design configurations from the similar design-metric map (not shown) for $r/a = 0.2$ and ΓM lattice termination.

The choice of $n_2 = 2.160$ is somewhat but not completely arbitrary—a choice of n_2 too close to $n_1 = n_e$ will tend to weight f_{PWE} more importantly than the fairly small change in θ_{v_g} . In contrast, an n_2 value widely different from n_1 will tend to overvalue $\Delta\theta_{v_g}$, since at least one of the two design conditions (n_1 or n_2) will not be near the band-edge.

For this value of $r/a = 0.2$ and termination along ΓK , Fig. 9 shows a number of interesting candidates where both strong ultra-refraction and low group velocity can be found in the same design configuration. We have picked out six such likely candidates (marked with white arrows in Fig. 9) and show the corresponding equifrequency contours with a representative superprism solution in parts (a–f) of Fig. 10. Fig. 10(g–i) shows three similar configurations found on the map for $r/a = 0.2$ but when the incoming light is incident upon a photonic crystal lattice terminated along ΓM (maps not shown). Note that for these latter three solutions, the conserved wavevector component is oriented at 90° with respect to earlier such equifrequency/superprism contours. Each superprism configuration is shown at an input angle and normalized frequency which makes the superprism behavior obvious at $n = 2.143$. However, one can realize the same functionality at a nearby r/a or incident angle, by slightly changing the index of refraction or the incident wavelength. Thus, even in the presence of some fabrication error, we should still have the opportunity to observe the efficiently tunable superprism effect.

To quantify this efficient tunability, we pick one particular configuration, near $\theta_{\text{in}} = 30.5^\circ$ and $\Omega = 0.320$, corresponding to Fig. 10(c). Shown in Fig. 11 is the group velocity angle as a function of refractive index for this configuration, shown at $\theta_{\text{in}} = 30.0^\circ$ and $\Omega = 0.320$ for $r/a = 0.2$ and ΓK termination. Note that because of the operation near the band-edge, a swing of $\sim 105^\circ$ is realized for a refractive index change of ~ 0.035 , or 65° for each 1% index change. This is already a 5-fold improvement in ultra-refraction over our first design. Shown in the inset of Fig. 11 are the out-of-plane electric field at two different index of refraction values obtained by 2D FDTD, with a input beam only slightly wider than used earlier ($10 \mu\text{m}$). The field enhancement within the photonic crystal structure is clear, and the anticipated beam-steering would be clearly visible in a near-field measurement (although less so in far-field).

Since this design configuration also has a larger field-factor, we can expect the scaling between index of refraction and applied electric field to follow the enhanced version of the Pockel’s equation (Eq. (3))

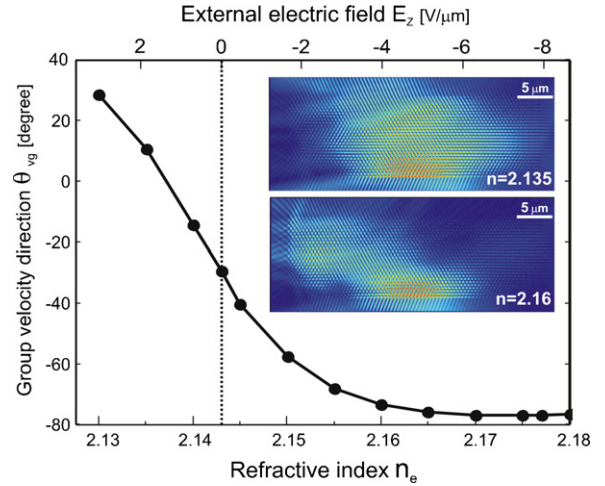


Fig. 11. Angle of the group velocity vector within a lithium niobate triangular lattice photonic crystal as a function of both refractive index n_e and external electric field E_z , for $r/a = 0.2$, $\theta_{\text{in}} = 30.0^\circ$, $\Omega = 0.32$, and ΓK termination (similar to Fig. 10(c)). Here the scaling from index change to electric field is performed with the slow-light enhanced Pockel’s equation, Eq. (3), with the local field factor taken to be $f = 3$. Considering the operation range from $n = 2.13$ to 2.165 , an angle change of $\sim 105^\circ$ occurs for a 1.63% change in index of refraction, yet requires only a change in external field of $8 \text{ V}/\mu\text{m}$. Insets show the out-of-plane electric field computed with 2D FDTD at two different indices of refraction, for an input beam of $10 \mu\text{m}$ width.

rather than the standard equation for bulk material (Eq. (2)). Given our still imperfect knowledge about the nature of the enhancement, quantifying the potential reduction in voltage requirements is somewhat tricky. To do so, we have chosen to use a value of $f = 3$. We make this choice as a tradeoff, one which is more conservative than the value of $f = 7$ found in our earlier experimental work on square-lattice photonic crystals [1,24]. We rationalize this because in that work, the light was propagating parallel to a Brillouin zone edge, where group velocities are known to become extremely low. However, this choice is slightly more aggressive than the f_{PWE} values calculated for this particular design point (which range from $f_{\text{PWE}} = 1.6$ – 2.0 within the main tuning range). This follows the observed relationship found in Ref. [24] that the f_{PWE} as calculated from group velocities is roughly 50% lower than the corresponding field factor value f obtained by integrating electric field within the structure (see also [27]).

In any case, this choice of $f = 3$ leads to a prediction that an angle swing of 105° would require a change in applied electric field of only $8 \text{ V}/\mu\text{m}$. For electrodes spaced at $13 \mu\text{m}$ as in Ref. [1,24], this would require 104 V , just slightly larger than the voltage changes used in that work. Comparing the angle-change per volt

between this configuration (Fig. 11) and our first (Fig. 4) which did not exploit slow light, we find that designing specifically for the slow-light enhancement of the electro-optic effect might be able to produce a 145-fold improvement in the efficiency of an appropriately designed electro-optically tunable active superprism.

The inherent cost in this design point is that at these kinds of locations within the dispersion diagram, the electro-optic enhancement can only be applied over a small bandwidth around the operating wavelength. This is because high local field factors are only found right near or at the band-edges. Visually, this is readily apparent in Fig. 9 because the design points showing strong ultra-refraction together with low group velocity all lie on narrow rim around the band-gap. In addition, the insets of Fig. 11 make it clear that the problems of efficient coupling into and out of the photonic crystal are only exacerbated by operation near the band-edge. Thus, there will be a strong trade-off between the efficiency of the tuning (a large angle-change per volt) and the other desirable aspects of the active superprism device (total angle-change, high operating bandwidth, low crosstalk, and low insertion loss).

Even though the design point shown in Fig. 11 is not necessarily more attractive than the one evaluated earlier (Figs. 3–7), there is still a very good reason to build and characterize it. Because the superprism effect can be measured independently under both wavelength and index change, the device shown in Fig. 11 would provide an excellent opportunity to provide further experimental data for understanding the electro-optic enhancement in nanostructured lithium niobate photonic crystals. For instance, one could directly compare the sensitivity of the angle deflection with voltage against the sensitivity with wavelength change at a constant voltage. This helps bypass a number of inherent experimental uncertainties that otherwise tend to complicate such a measurement. The testing of superprism devices designed to operate at various degrees of proximity to the band-edge can help complete our understanding of the enhanced electro-optic effect. Then, we can better quantify the tradeoff between increased efficiency and the loss of operating bandwidth, allowing us to pick an optimal design point that is close but not “too close” to the band-edge.

Thus, the next logical steps for future research are to extend the procedure developed here to the case of in-plane polarization, and then to fabricate a suitable device using an annealed-proton exchanged (APE) lithium niobate waveguide. An APE (rather than diffused titanium) waveguide will help keep the optical mode closer to the surface, providing better

overlap with cylindrical holes of finite depth (as fabricated by milling with a focused ion beam). It may also be useful to fabricate such a photonic crystal in a deep trench etched into the substrate surface, in order to force the mode to interact with the holes and to more easily observe this interaction with a near-field optical probe. With such a fabricated device, one can experimentally verify the presence and magnitude of this enhanced superprism effect, and then feed new information obtained via experiment back into subsequent designs.

6. Conclusions

An active photonic crystal superprism device using the electro-optic effect in lithium niobate would be an extremely attractive device for the future realization of ultra-fast, ultra-compact optical components for optical processing and interconnect. In contrast to previous passive multiplexer designs, we propose a novel active superprism device which implements a three-port tunable bandpass filter. We illustrate the operation of this device over a reasonable bandwidth using 2D FDTD numerical simulations. In order to improve the voltage-tuning efficiency of the device, we introduce a methodology for visualizing the design space represented by extensive plane-wave expansion results. This procedure readily identifies designs that combine both strong ultra-refraction and low group velocity. We theoretically predict that the slow-light enhancement of the electro-optic effect in lithium niobate could potentially increase the angle-change per volt by a factor of 145 over designs that rely on ultra-refraction alone. However, we observe that operation too close to the band-edge sacrifices many of the other desirable aspects of the active superprism device. Experimental characterization of such near-band-edge superprism devices will be a critical step towards better quantitative understanding of this slow-light enhancement in lithium niobate. In turn, this will then enable quantitative assessment of the tradeoff between voltage efficiency and operating bandwidth, leading to efficiently tunable and high-performance active superprism devices.

Acknowledgments

The authors want to thank INTERREG III (“CRISLAR”) for financial support. GWB would like to thank the CNRS and IBM management for making his extended visit to FEMTO-ST in Besançon possible.

References

- [1] M. Roussey, M.-P. Bernal, N. Courjal, D. Van Labeke, F.I. Baida, Electro-optic effect exaltation on lithium niobate photonic crystals due to slow photons, *Appl. Phys. Lett.* 89 (24) (2006) 241110.
- [2] J.D. Joannopoulos, R.D. Meade, J.N. Winn, *Photonic Crystals: Molding the Flow of Light*, Princeton University Press, Princeton, NJ, 1995.
- [3] J.D. Joannopoulos, P.R. Villeneuve, S.H. Fan, Photonic crystals: Putting a new twist on light, *Nature* 386 (6621) (1997) 143–149.
- [4] O. Painter, R.K. Lee, A. Scherer, A. Yariv, J.D. O'Brien, P.D. Dapkus, I. Kim, Two-dimensional photonic band-gap defect mode laser, *Science* 284 (5421) (1999) 1819–1821.
- [5] S.Y. Lin, V.M. Hietala, L. Wang, E.D. Jones, Highly dispersive photonic band-gap prism, *Opt. Lett.* 21 (21) (1996) 1771–1773.
- [6] H. Kosaka, T. Kawashima, A. Tomita, M. Notomi, T. Tamamura, T. Sato, S. Kawakami, Superprism phenomena in photonic crystals, *Phys. Rev. B* 58 (16) (1998) R10096–R10099.
- [7] B. Gralak, S. Enoch, G. Tayeb, Anomalous refractive properties of photonic crystals, *J. Opt. Soc. Am. A* 17 (6) (2000) 1012–1020.
- [8] X. Hu, C.T. Chan, Photonic crystals with silver nanowires as a near-infrared superlens, *Appl. Phys. Lett.* 85 (9) (2004) 1520–1522.
- [9] R.A. Shelby, D.R. Smith, S. Schultz, Experimental verification of a negative index of refraction, *Science* 292 (5514) (2001) 77–79.
- [10] A. Lupu, E. Cassan, S. Laval, L. El Melhaoui, P. Lyan, J.M. Fedeli, Experimental evidence for superprism phenomena in soi photonic crystals, *Opt. Exp.* 12 (23) (2004) 5690–5696.
- [11] T. Matsumoto, S. Fujita, T. Baba, Wavelength demultiplexer consisting of photonic crystal superprism and superlens, *Opt. Exp.* 13 (26) (2005) 10768–10776.
- [12] D. Scrymgeour, N. Malkova, V. Sungwon Kim, Gopalan, Electro optic control of the superprism effect in photonic crystals, *Appl. Phys. Lett.* 82 (19) (2003) 3176–3178.
- [13] S. Xiong, H. Fukushima, Analysis of light propagation in index tunable photonic crystals, *J. Appl. Phys.* 94 (2) (2003) 1286–1288.
- [14] G. Alagappan, X.W. Sun, M.B. Yu, P. Shum, D. den Engelsen, Tunable dispersion properties of liquid crystal infiltrated into a two-dimensional photonic crystal, *IEEE J. Quant. Electr.* 42 (3/4) (2006) 404–409.
- [15] N.C. Panoiu, M. Bahl, R.M. Osgood, Optically tunable superprism effect in nonlinear photonic crystals, *Opt. Lett.* 28 (24) (2003) 2503–2505.
- [16] T. Baba, T. Matsumoto, Resolution of photonic crystal superprism, *Appl. Phys. Lett.* 81 (13) (2002) 2325–2327.
- [17] J. Witzens, T. Baehr-Jones, A. Scherer, Hybrid superprism with low insertion losses and suppressed cross-talk, *Phys. Rev. E* 71 (2) (2005) 026604.
- [18] B. Momeni, A. Adibi, Optimization of photonic crystal demultiplexers based on the superprism effect, *Appl. Phys. B* 77 (6–7) (2003) 555–560.
- [19] L. Arizmendi, Photonic applications of lithium niobate crystals, *Phys. Stat. Sol. A* 201 (2) (2004) 253–283.
- [20] F. Lacour, N. Courjal, M.P. Bernal, A. Sabac, C. Bainier, M. Spajer, Nanostructuring lithium niobate substrates by focused ion beam milling, *Opt. Mater.* 27 (8) (2005) 1421–1425.
- [21] M. Roussey, M.P. Bernal, N. Courjal, F.I. Baida, Experimental and theoretical characterization of a lithium niobate photonic crystal, *Appl. Phys. Lett.* 87 (24) (2005) 241101.
- [22] R.S. Weis, T.K. Gaylord, Lithium niobate: summary of physical properties and crystal structure, *Appl. Phys. A* 37 (1985) 191–203.
- [23] R.W. Boyd, *Nonlinear Optics*, Academic Press, 2003.
- [24] M. Roussey, F.I. Baida, M.-P. Bernal, Experimental and theoretical observation of the slow light effect on a tunable photonic crystal, *J. Opt. Soc. Am. B* 24 (6) (2007) 1416–1422.
- [25] R. Frey, P. Delaye, G. Roosen, Non-linéarités optiques du troisième ordre dans les cristaux photoniques, in: H. Rigneault, J.-M. Lourtioz, C. Delalande, A. Levenson (Eds.), *La nanophotonique*, Collection Technique et Scientifique des Télécommunications, GET et Lavoisier, Paris, 2005, pp. 207–222.
- [26] P. Delaye, M. Astic, R. Frey, G. Roosen, Transfer-matrix modeling of four-wave mixing at the band edge of a one-dimensional photonic crystal, *J. Opt. Soc. Am. B* 22 (11) (2005) 2494–2504.
- [27] Note that we have identified two minor errors in Ref. [24] which pertain to the comparison between local field factor f obtained from integration of electric field and the approximate local field factor f_{PWE} calculated from the group velocity. Due to a minor typographical error, the y-label of Fig. 5 in that paper indicates group velocities that are $1000 \times$ too small. As a result, the value of $f_{PWE} \sim 94$ given in the text below this figure is too large by the square root of 1000. The actual value of $f_{PWE} \sim 2.97$ is thus significantly smaller than the value of f calculated from FDTD (Fig. 6 of Ref. [24] gives $f \sim 4.8$, and Fig. 7b shows f values as large as 7).
- [28] M.M. Abouelleil, F.J. Leonberger, Wave-guides in lithium-niobate, *J. Am. Ceram. Soc.* 72 (8) (1989) 1311–1321.
- [29] S.P. Guo, S. Albin, Simple plane wave implementation for photonic crystal calculations, *Opt. Exp.* 11 (2) (2003) 167–175.
- [30] BandSolve 3.0, RSoft Design Group, 2006.
- [31] M. Notomi, Theory of light propagation in strongly modulated photonic crystals: refraction like behavior in the vicinity of the photonic band gap, *Phys. Rev. B* 62 (16) (2000) 10696–10705.
- [32] H. Kosaka, T. Kawashima, A. Tomita, M. Notomi, T. Tamamura, T. Sato, S. Kawakami, Photonic crystals for micro lightwave circuits using wavelength-dependent angular beam steering, *Appl. Phys. Lett.* 74 (10) (1999) 1370–1372.
- [33] L.J. Wu, M. Mazilu, T. Karle, T.F. Krauss, Superprism phenomena in planar photonic crystals, *IEEE J. Quant. Electr.* 38 (7) (2002) 915–918.
- [34] J.J. Baumberg, N.M.B. Perney, M.C. Netti, M.D.C. Charlton, M. Zoorob, G.J. Parker, Visible-wavelength super-refraction in photonic crystal superprisms, *Appl. Phys. Lett.* 85 (3) (2004) 354–356.
- [35] A. Taflove, S.C. Hagness, *Computational Electrodynamics: The Finite-difference Time-domain Method*, 3rd ed., Artech House, Boston, 2005.
- [36] T. Baba, T. Matsumoto, M. Echizen, Finite difference time domain study of high efficiency photonic crystal superprisms, *Opt. Exp.* 12 (19) (2004) 4608–4613.